Engineering Fracture Mechanics 307 (2024) 110320

Contents lists available at ScienceDirect

Engineering Fracture Mechanics

journal homepage: www.elsevier.com/locate/engfracmech

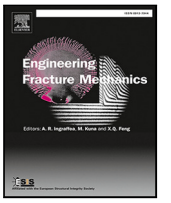

Modified double cantilever beam test method for mode-I energy release rate of elastic adhesive layers

Tetsuya Morimoto [a,*], Hisaya Katoh [a], Yuichi Ishida [a], Eiichi Hara [a], Masahiro Kusano [b], Kimiyoshi Naito [b], Makoto Watanabe [b], Kiyoka Takagi [c], Keiji Arai [c], Koichi Hasegawa [c]

[a] Japan Aerospace Exploration Agency (JAXA), 6-13-1 Osawa, Mitaka -City, 181-0015, Tokyo, Japan
[b] National Institute for Materials Science (NIMS), 1-2-1 Sengen, Tsukuba-City, 305-0047, Ibaraki, Japan
[c] Mitsubishi Heavy Industries, Ltd. (MHI), 1 Toyoba, Toyoyama-Cho, Nishikasugai-gun, 480-0293, Aichi, Japan

ARTICLE INFO

Keywords:
DCB test
Adhesive layer
Elasticity
Winkler's foundation
Energy release rate
Bernulli–Euler beam

ABSTRACT

This study proposes a Mode I double cantilever beam (DCB) test method for debonding thick elastic adhesive layers. The approach integrates Bernoulli–Euler beams connected via spring elements akin to Winkler's foundation. Energy release rate determination considers crack length correlation with elastic deformation in the crack-front region, accounting for both beam rotation and lateral movement. Evaluation of Ti6Al4V samples bonded with FM 309 adhesive revealed higher initial energy release rates with the conventional beam theory and conservative values with the modified beam theory. The proposed method offered improved consistency, and less conservative energy release rate values compared to the modified theory.

1. Introduction

The reliability of adhesive bonding in passenger aircraft structures have been debated, necessitating a classical design supplemented with fastening in bonding joints [1,2]. In particular, the case of Air Transat Flight 961 "Loss of Rudder in flight" in 2005 was found to be caused by "Weak Bond", which is an unexpected loss of bonding performance, resulting in increased doubts about the reliability of adhesive bonding [3]. Based on the status of adhesive bonding in aircraft structures, the Federal Aviation Administration (FAA), USA, had established an international working group on metallic and composite structures for airplanes suitable for air transport operations, and had finalized its recommendations in the "Transport Airplane Metallic and Composite Structures Working Group – Final Recommendation Report on Structural Bonding [4]". This recommendation report proposes a change in the adhesion-related sections of FAA Advisory Circular 20-107B "COMPOSITE AIRCRAFT STRUCTURE" as general visual inspection (GVI) is considered inadequate to detect bond failure; the most effective methods, including detailed visual inspection (DVI) and non-destructive testing using equipment, should be applied to inspect the flange side edge of the bonded area [5]. In addition, it has been reported that local peel forces or Mode I loadings exist in the stress distribution of bonded joints, whereas most bonded joints and attachments are designed primarily to transfer shear loads. Therefore, a test method is required to assess whether adequate visual inspection or non-destructive testing is applied to cracks along the bonded line under Mode I loading conditions. These basic data are essential for designing adhesive joints in aircraft applications.

Double cantilever beam (DCB) test is a potential candidate as it is a simple yet powerful method to investigate mode I energy release associated with crack propagation through an interface between two plate coupons. Moreover, it is already standardized by

* Corresponding author.
E-mail address: morimoto.tetsuya@jaxa.jp (T. Morimoto).

https://doi.org/10.1016/j.engfracmech.2024.110320
Received 29 March 2024; Received in revised form 13 July 2024; Accepted 15 July 2024
Available online 20 July 2024

Nomenclature

A_i	Integral constants or analytical coefficients
B_i	Integral constants or analytical coefficients
BT	Beam theory
CF	Correlation factor
DVI	Detailed Visual Inspection
E	Young's modulus
E_B	Young's modulus of the beam
E_F	Young's modulus of the foundation
Erf	Error function
$f(x)$	Deflection function of the beam
$f_C(x)$	Lateral position of the cracked section
G	Energy release rates
G_{DCB}	Energy release rate in the DCB test form
GVI	General Visual Inspection
I	Moment of inertia of the area
L	Hinge loading-arm length
l	Crack length
l_i	i th data of crack length
M	Moment
M_C	Moment at the crack tip
MBT	Modified beam theory
P	Lateral load
P_C	Lateral load at the crack tip
R_{BT}	Selection parameter for beam theory
R_{MBT}	Selection parameter for modified beam theory
S.D.	Standard Deviation
t	Thickness
t_{DCB}	Adhesive thickness of DCB test sample
t_B	Beam thickness
t_F	Thickness of the Winkler's foundation
U	Strain energy of the beam
w	Beam width
x	Distance along beam from tip
α	Converted coefficients
$1/\alpha$	Proposed crack-length correlation factor
β	Integration constants
λ	Compliance
λ_i	ith data of compliance
χ	Crack length correlation factor
δ	Crack opening displacements
Δ	Crack length correlation factor of the modified beam theory

the International Organization for Standardization (ISO) 15024, American Society for Testing and Materials (ASTM) D5528, D3433, and Japanese Industrial Standards (JIS) K7086. Additionally, it is widely used to obtain the energy release rate values of mode I delamination for thin layers such as laminated composite materials [6–9]. The current DCB test standards set the scope for a crack to extend through a thin interface; thus, elastic deformation can be ignored. Therefore, there is no lateral deformation of the beam cross-section at the crack front, and the beam region where the crack does not extend shows no deformation. However, as reported by Akhavan-Safar et al. for the mode I fracture toughness of adhesive layers [10], in adhesive layers where the thickness is not negligible, as is often the case in engineering applications, it is questionable whether the energy release rate obtained from the DCB test corresponds to the fracture toughness of the adhesive. Therefore, the scope of DCB test standards should be widened to include cases for the elastic layer of non-negligible thickness causing rotation and lateral deformation of the beam cross-section at the crack front and deformation of the region where the crack has not yet extended.

The theoretical background of the present DCB test was a Bernoulli–Euler beam with fixed and free ends, assuming loading perpendicular to the longitudinal direction of the beam. Bisshopp et al. derived an exact solution for the bending displacement of a single beam using an elliptical function and showed that the difference between the bending of a Bernoulli–Euler beam and the exact solution was within a negligible range when the bending displacement was less than 20% of the beam length.[11]. Based on

this solution, Devitt et al. determined the fracture toughness in the form of an implicit function and verified it for E-glass fiber-reinforced epoxy laminates using a fracture toughness test method; for this, they applied a devised jig to reduce the errors caused by the moment generated by the hinge loading arm [12]. Ashizawa et al. devised a hinged double-cantilever beam test method to minimize the moment [13].

Contrarily, under increased loading, owing to the development of toughened epoxy resins, some moments become significant because of the increased hinge loading arm of the high-load hinge. Moreover, the exact solution as an implicit function requires a numerical table for the normalized parameters. These requirements can render engineering applications challenging. Therefore, Wang et al. derived an approximation formula that considers the effect of the hinge loading arm as an explicit function using series expansion [14] and derived a rigorous solution that considers the effect of the hinge loading arm by adding a correction term to the Bernoulli–Euler beam theory [15]. Thus, it is practical to establish a DCB test method. In test standards, such as ASTM D5528 and ISO 15024, the correction formula proposed by Williams [15] and the calculation formula for approximating the compliance and crack length proposed by Berry using the nth power law [16] were presented, and the selection was assigned to the users. To establish the DCB test standard JIS K7086 for carbon fiber-reinforced plastic (CFRP) interlaminar fracture toughness, Kageyama et al. assumed that the elastic deformation of the crack propagation area is negligible for thin and highly rigid interlaminar CFRP. They verified this assumption through comparisons with mechanical tests and finite-element analyses [17–20].

However, when delamination occurs through thick elastic layers such as in adhesive joints, the present DCB test standards may yield inaccurate results because of the opening and rotation at the crack tip induced by deformation across the uncracked elastic layer. Therefore, an elastic beam on top of an elastic layer was investigated because of its unique bending behavior under various loading conditions. Winkler developed a solution for Bernoulli–Euler beam bending for civil engineering applications, such as railroad tracks on sleepers, assuming that the reaction of a point on the foundation solely depends on the settlement and that the point is independent of the settlements of neighboring points [21,22]. For the elastic foundation model, Biot proposed an exact solution for an infinite Bernoulli–Euler beam under a sine wave and concentrated loading, which produced a bending moment, as in the case of an uncracked elastic layer in the DCB test [23]. Pavlović et al. analyzed a Bernoulli–Euler beam that was not fixed to Winkler's elastic foundation, as is the case with cracked sections. Thus, the beam sections deflected from the foundation are independent of the foundation-based loading [24].

Kanninen investigated the crack propagation in DCB test specimens of isotropic materials by assuming a finite-length beam partly supported by a Pasternak elastic foundation with elasticities of both deflection and rotation [25,26]. The rotational distortion at the crack end was considered in the analyses, and it was concluded that a beam with shear distortion in the Timoshenko beam theory can predict the numerical results. Regarding the shear distortion of an isotropic beam, Whitney employed the higher-order shear deformation plate theory for accurate stress distribution analysis of a DCB test specimen [27]. By extending the Kanninen models, Williams provided a factor for the crack length correction of an orthotropic beam rotating at the crack end on a Pasternak elastic foundation [28] and derived expressions for the energy release rate [29]. Kondo analyzed DCB specimens using a Timoshenko beam supported by a Winkler foundation and concluded that the analyses accurately correlated with the predictions of Whitney [27] compared to finite element analyses [30]. Shokrieh et al. comparatively investigated DCB analyses that considered transverse shear deformation in beams and root rotation at the crack tip [31]. Takeda developed a new model to provide the effective crack length and compared it with a wedge test for the energy release rate of adhesive bonds, showing consistent results. Subsequently, they demonstrated the applicability of the wedge test and a new model for an environmental test of bonding on the mode I energy release rate [32].

These solutions of the modified beam theory (MBT) yielded crack-length correlation factors focusing on the shear deformation or rotation at the crack front in beams, which are often derived through linear fitting between $Compliance^{1/3}$ and the crack length, assuming that the factors are small compared to the crack length [6,7,9]. However, in aircraft design, it is crucial to confirm whether the correlation length is acceptably small compared to the measured crack length. This consideration arises because factors related to the thickness and elasticity of the foundation are expected to increase the influence of slender beams on thick and elastic foundations, similar to the behavior observed in elastic adhesives applications for thin elastic materials such as advanced CFRPs. Although advanced numerical methods display improved agreement with the data of the energy release rate, showing promising potential for engineering design applications of adhesive joints [33,34], the importance of input parameters using mechanical testing increases in these applications; thus, a modification of the present DCB test methods is required to derive data on elastic adhesive layers of non-negligible thickness.

Therefore, in this study, we considered the infinitesimal deformation of a slender beam on an elastic foundation, assuming that the beam deformation is within a predictable level using the Bernoulli–Euler beam model, and that both the crack end rotation and lateral movement are given by Winkler's elastic foundation model. This approach separated the beam into cracked and foundation-top sections. We set the loading conditions as the deflectional load and moment at the end of the cracked section and linearly connected the other end to the top section of the foundation. The deflectional load was multiplied by the crack-length-added moment loading for the foundation-top section. The deflection and rotation at the connecting point were provided with a known solution to Winkler's elastic foundation model. We predicted the deflection at the loading end of the cracked section by superimposing the connecting-point deflection, slope deflection using the connecting-point rotation and crack length, and the deformation of the cracked section using both the deflectional load and moment. The derived solution yielded an energy release rate with a foundation-based correlation factor for crack length.

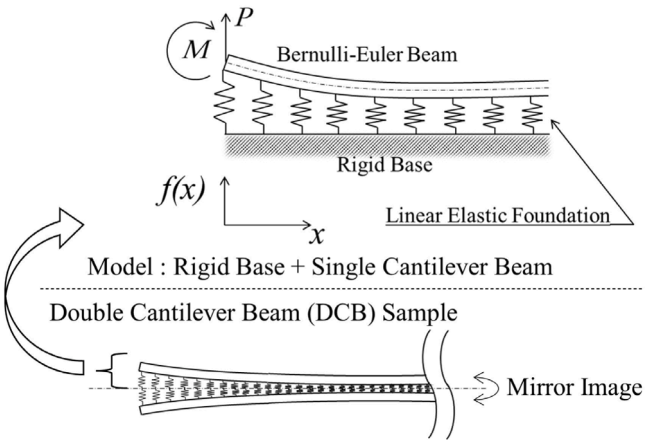

Fig. 1. Winkler's linear elastic foundation model.

2. Calculations of delamination in elastic foundation

2.1. Lateral bending of single cantilever beam on an elastic foundation

The DCB test sample had a mirror-image relationship with a plane of symmetry in the center because it was fabricated by joining two identical cantilevers (Fig. 1). Therefore, the model with a single cantilever and rigid base represents half of the entire DCB sample. Assuming that the reaction of the modeled upper half of the DCB sample in a single cantilever form is proportional to the settlement and that the array of points forms a linear elastic foundation, the bending of the beam can be expressed as follows:

$$E_B I \frac{d^4 f(x)}{dx^4} = -\frac{E_F w}{t_F} f(x) \tag{1}$$

where E_B is Young's modulus of the beam, I is the moment of inertia of the beam area, $f(x)$ is the positive beam deflection function in the upper direction, x is the distance from the tip of the beam, E_F is Young's modulus of the elastic foundation, t_F is the thickness of the elastic foundation, and w is the width of the beam. The thickness of the elastic foundation in the DCB test sample t_{DCB} was twice that of t_F.

$$t_{DCB} = 2t_F. \tag{2}$$

Eq. 1 can be rewritten as Eq. (4), which yields α in Eqs. (3).

$$\alpha = \left(\frac{E_F w}{4 E_B I t_F} \right)^{\frac{1}{4}} \tag{3}$$

$$\frac{d^4 f(x)}{dx^4} = -4\alpha^4 f(x) \tag{4}$$

When the lateral loading P and moment M are applied at tip $x = 0$, the complementary solution is expressed as follows: By setting $f(x) = e^{\beta x}$, Eq. (4) yields the following relationship:

$$\beta = \pm(1 \pm i)\alpha, \tag{5}$$

where β is an integral constant. Therefore, $f(x)$ can be expressed using the integral constant A_i as follows:

$$f(x) = A_1 e^{(1+i)\alpha x} + A_2 e^{(1-i)\alpha x} + A_3 e^{-(1+i)\alpha x} + A_4 e^{-(1-i)\alpha x} \tag{6}$$

Eq. (6) is expressed using integral constants B_i by applying the relationships $e^{ix} - e^{-ix} = 2i\sin(x)$ and $e^{ix} + e^{-ix} = 2i\cos(x)$:

$$f(x) = e^{\alpha x}\{B_1 \cos(\alpha x) + B_2 \sin(\alpha x)\} + e^{-\alpha x}\{B_3 \cos(\alpha x) + B_4 \sin(\alpha x)\} \tag{7}$$

The modeled cantilever shown in Fig. 1 converges to $f(x) = 0$. in $x \to \infty$, which yields $B_1 = B_2 = 0$. Therefore, Eq. (7) yields the following relationship:

$$\frac{\partial^2 f(x)}{\partial x^2} = -2\alpha^2 e^{-\alpha x}\{B_4 \cos(\alpha x) - B_3 \sin(\alpha x)\} \tag{8}$$

$$\frac{\partial^3 f(x)}{\partial x^3} = 2\alpha^3 e^{-\alpha x}\{(B_3 + B_4)\cos(\alpha x) - (B_3 - B_4)\sin(\alpha x)\} \tag{9}$$

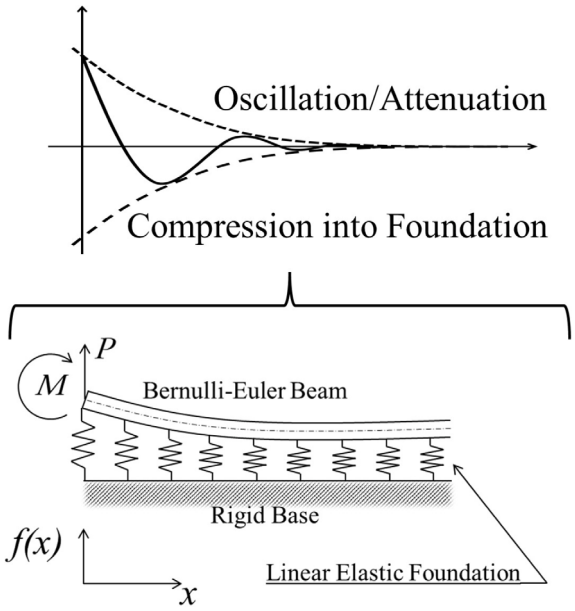

Fig. 2. Beam deflection atop Winkler's Foundation.

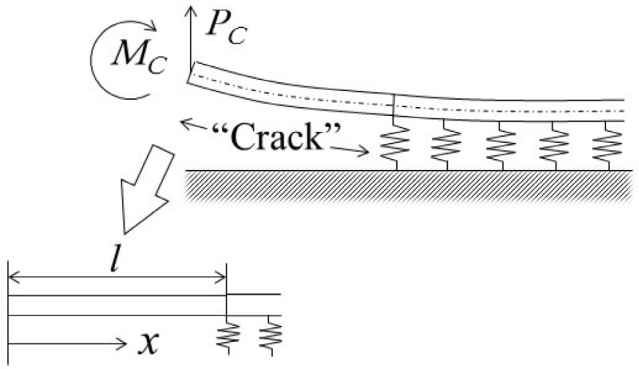

Fig. 3. Cracked section at the tip of Winkler's Foundation.

Furthermore, loadings M and P at $x = 0$ lead to the following relationships when deflection function $f(x)$ of the beam is positive in the upper direction.

$$E_B I \left[\frac{\partial^2 f(x)}{\partial x^2}\right]_{x=0} = M \tag{10}$$

$$E_B I \left[\frac{\partial^3 f(x)}{\partial x^3}\right]_{x=0} = P \tag{11}$$

Thereby, Eq. (7) yields the following relationship.

$$f(x) = \frac{e^{-\alpha x}}{2E_B I \alpha^3}[P\cos(\alpha x) + M\alpha\{\cos(\alpha x) - \sin(\alpha x)\}] \tag{12}$$

Eq. (12) gives the beam deflection, as shown in Fig. 2, indicating compression into the foundation near the tip $x = 0$.

2.2. Lateral bending of single cantilever beam on an elastic foundation with cracked section

Assume that a beam of length l made of identical material with an identical cross-sectional shape is connected to the tip of this beam; however, it is not connected to the elastic foundation to represent the cracked section (see Figs. 3 and 4).

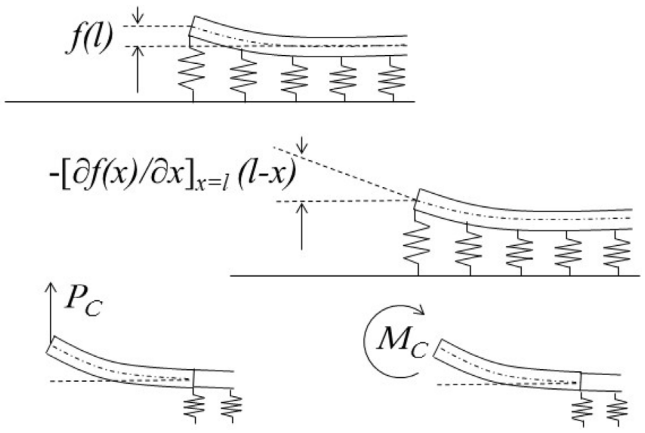

Fig. 4. Lateral movements at the cracked section.

The lateral bending of the foundation-top section $f(x), l \le x$ is revised as follows:

$$f(x) = \frac{e^{-\alpha(x-l)}}{2E_B I\alpha^3}\langle P_C \cos\{\alpha(x-l)\} + (M_C + P_C l)\alpha[\cos\{\alpha(x-l)\} - \sin\{\alpha(x-l)\}]\rangle \tag{13}$$

The lateral position of the cracked section $f_C(x), 0 \le x < l$, in the form of the sum of the lateral movement at the crack end is expressed as follows $f(l)$, slope height $-\left[\frac{\partial f(x)}{\partial x}\right]_{x=l}(l-x)$, and bendings at the cracked section caused by the loading P_C and moment M_C:

$$f_C(x) = f(l) - \left[\frac{\partial f(x)}{\partial x}\right]_{x=l}(l-x) + \frac{P_C}{6E_B I}(x^3 - 3l^2x + 2l^3) + \frac{M_C}{2E_B I}(x^2 - 2lx + l^2) \tag{14}$$

Where,

$$f(l) = \frac{1}{2E_B I\alpha^3}\{P_C + (M_C + P_C l)\alpha\}, \tag{15}$$

and

$$\begin{aligned}\frac{\partial f(x)}{\partial x} &= -\frac{e^{-\alpha(x-l)}}{2E_B I\alpha^2}\langle P_C \cos\{\alpha(x-l)\} + (M_C + P_C l)\alpha[\cos\{\alpha(x-l)\} - \sin\{\alpha(x-l)\}]\rangle \\ &-\frac{e^{-\alpha(x-l)}}{2E_B I\alpha^2}\langle P_C \sin\{\alpha(x-l)\} + (M_C + P_C l)\alpha[\sin\{\alpha(x-l)\} + \cos\{\alpha(x-l)\}]\rangle \\ &= -\frac{e^{-\alpha(x-l)}}{2E_B I\alpha^2}\langle P_C[\cos\{\alpha(x-l)\} + \sin\{\alpha(x-l)\}] + 2(M_C + P_C l)\alpha\cos\{\alpha(x-l)\}\rangle,\end{aligned} \tag{16}$$

thus,

$$\left[\frac{\partial f(x)}{\partial x}\right]_{x=l} = -\frac{1}{2E_B I\alpha^2}\{P_C + 2\alpha(M_C + P_C l)\}. \tag{17}$$

Therefore, the lateral position $f_C(x)$ at the loading point $x = 0$ can be expressed as follows:

$$\begin{aligned}f_C(0) &= \frac{1}{2E_B I\alpha^3}\{P_C + \alpha(M_C + P_C l)\} + \frac{1}{2E_B I\alpha^2}\{P_C + 2\alpha(M_C + P_C l)\}l + \frac{P_C l^3}{3E_B I} + \frac{M_C l^2}{2E_B I} \\ &= \frac{1}{6E_B I}\left[P_C\left\{2\left(\frac{1}{\alpha} + l\right)^3 + \frac{1}{\alpha^3}\right\} + 3M_C\left(\frac{1}{\alpha} + l\right)^2\right]\end{aligned} \tag{18}$$

2.3. Calculation of energy release rate

The strain energy U of the beam in Eq. (18) can be expressed as

$$U = U(P_C, M_C, l) = \frac{1}{2}\left\{P_C f_C(0) - M_C\left[\frac{\partial f_C(x)}{\partial x}\right]_{x=0}\right\} \tag{19}$$

The differential of $U(P_C, M_C, l)$ can be expressed as:

$$dU = \frac{\partial U}{\partial P_C}dP_C + \frac{\partial U}{\partial M_C}dM_C + \frac{\partial U}{\partial l}dl \tag{20}$$

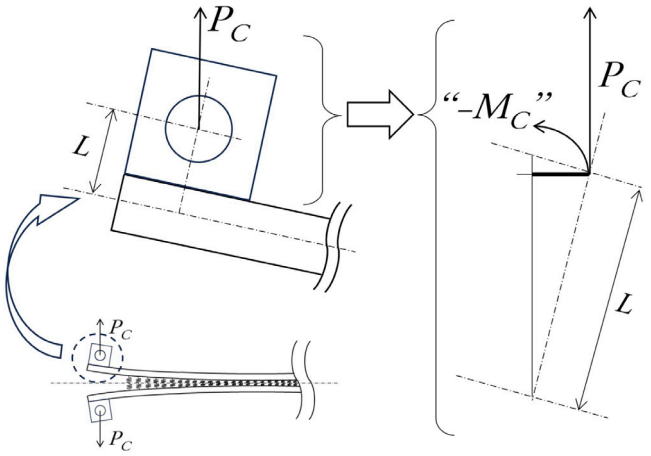

Fig. 5. Moment by the hinge loading arm.

Therefore, for the case in which the crack length l slightly extends to $l+dl$, differential $dU_{l\to l+dl}$ at $f_C(0)$ is expressed as follows:

$$dU_{l\to l+dl} = \frac{1}{2}\left\{ P_C \frac{\partial f_C(0)}{\partial l} dl - M_C \frac{\partial \left[\frac{\partial f_C(x)}{\partial x}\right]_{x=0}}{\partial l} dl \right\} \tag{21}$$

Eq. (18) yields the following relationship:

$$\frac{\partial f_C(0)}{\partial l} = \frac{1}{E_B I \alpha^2}\{P_C + \alpha(M_C + 2P_C l)\} + \frac{P_C l^2}{E_B I} + \frac{M_C l}{E_B I} \tag{22}$$

Furthermore,

$$\frac{\partial f_C(x)}{\partial x} = \left[\frac{\partial f(x)}{\partial x}\right]_{x=l} + \frac{P_C}{2E_B I}(x^2 - l^2) + \frac{M_C}{E_B I}(x - l), \tag{23}$$

thus,

$$\left[\frac{\partial f_C(x)}{\partial x}\right]_{x=0} = -\frac{1}{2E_B I \alpha^2}\{P_C + 2\alpha(M_C + P_C l)\} - \frac{P_C}{2E_B I} l^2 - \frac{M_C}{E_B I} l, \tag{24}$$

providing

$$\frac{\partial \left[\frac{\partial f_C(x)}{\partial x}\right]_{x=0}}{\partial l} = -\frac{P_C}{E_B I \alpha} - \frac{P_C}{E_B I} l - \frac{M_C}{E_B I}. \tag{25}$$

Therefore, the energy release rate $G = dU_{l\to l+dl}/wdl$ is given by

$$\begin{aligned} G &= \frac{dU_{l\to l+dl}}{wdl} \\ &= P_C \frac{\partial f_C(0)}{2w\partial l} - M_C \frac{\partial \left[\frac{\partial f_C(x)}{\partial x}\right]_{x=0}}{2w\partial l} \\ &= \frac{P_C}{2w}\left[\frac{1}{E_B I \alpha^2}\{P_C + \alpha(M_C + 2P_C l)\} + \frac{P_C l^2}{E_B I} + \frac{M_C l}{E_B I}\right] + \frac{M_C}{2w}\left(\frac{P_C}{E_B I \alpha} + \frac{P_C}{E_B I} l + \frac{M_C}{E_B I}\right) \\ &= \frac{1}{2wE_B I}\left\{P_C\left(\frac{1}{\alpha} + l\right) + M_C\right\}^2 \end{aligned} \tag{26}$$

2.4. Moment by hinge loading arm

The moment load is induced by the lateral loading P_C when the hinge loading arm L is non-negligible because of the loading-block configuration, as shown in Fig. 5.

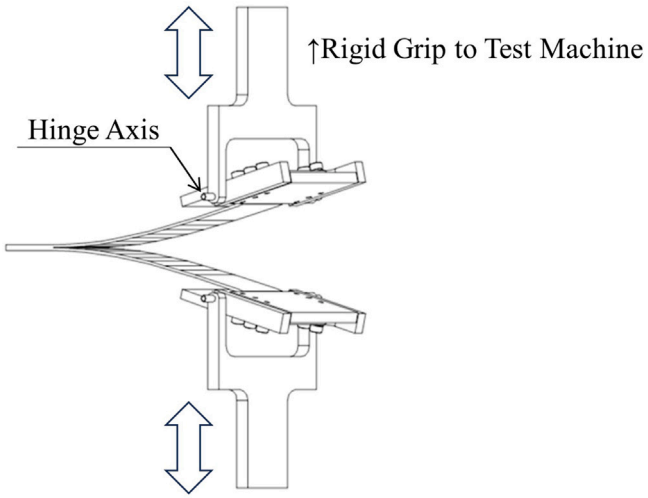

Fig. 6. ISO 15024 loading hinge setup for DCB Test.

The induced moment M_C is expressed as follows when slope $\left[\frac{\partial f_C(x)}{\partial x}\right]_{x=0}$ is close to 0:

$$M_C = -\left[\frac{\partial f_C(x)}{\partial x}\right]_{x=0} LP_C \tag{27}$$

The following relationship is obtained by applying Eqs. (24) and (27) for $\left[\frac{\partial f_C(x)}{\partial x}\right]_{x=0}$

$$-\frac{M_C}{LP_C} = \frac{1}{2E_B I}\left\{P_C\left(\frac{1}{\alpha}+l\right)^2 + 2M_C\left(\frac{1}{\alpha}+l\right)\right\} \tag{28}$$

Therefore, moment M_C is expressed as follows:

$$M_C = -\frac{{P_C}^2\left(\frac{1}{\alpha}+l\right)^2 L}{2\{E_B I + (\frac{1}{\alpha}+l)LP_C\}} \tag{29}$$

2.5. Energy release rate in DCB test

Eqs. (26) and (29) yields the following relationship for the energy release rate:

$$\begin{aligned} G &= \frac{{P_C}^2}{2wE_B I}\left[\left(\frac{1}{\alpha}+l\right) - \frac{{P_C}^2\left(\frac{1}{\alpha}+l\right)^2 L}{2\{E_B I + (\frac{1}{\alpha}+l)LP_C\}}\right]^2 \\ &= \frac{{P_C}^2}{2wE_B I}\left[\frac{\left(\frac{1}{\alpha}+l\right)\left\{2+\left(\frac{1}{\alpha}+l\right)\frac{LP_C}{E_B I}\right\}}{2\left\{1+\left(\frac{1}{\alpha}+l\right)\frac{LP_C}{E_B I}\right\}}\right]^2 \end{aligned} \tag{30}$$

For the DCB test case, the energy release rate G_{DCB} was twice that of the single-cantilever model G in Eq. (30), yielding

$$G_{DCB} = 2\times G = \frac{{P_C}^2}{wE_B I}\left[\frac{\left(\frac{1}{\alpha}+l\right)\left\{2+\left(\frac{1}{\alpha}+l\right)\frac{LP_C}{E_B I}\right\}}{2\left\{1+\left(\frac{1}{\alpha}+l\right)\frac{LP_C}{E_B I}\right\}}\right]^2. \tag{31}$$

For extreme cases of the hinge loading arm L, where $L = 0$, Eq. (31) can be simplified as follows:

$$G_{DCB,L\to 0} = \frac{{P_C}^2}{wE_B I}\left(\frac{1}{\alpha}+l\right)^2 \tag{32}$$

Eq. (32) is attained when the axis center of the loading hinge is set to the middle of the plate thickness, as standardized in ISO 15024 (see Fig. 6).

With Eq. (3), $1/\alpha$ in Eq. (32) appears negligible when the adhesive is rigid compared to the beam as $E_F \gg E_B$, or the thickness is small as $t_F \to 0$. However, for the elastic adhesives with $E_F \approx E_B$, the thickness appears to be an important factor that affects

the accuracy of the energy release rate in Eq. (32). For example, a DCB test with rectangular cross-sectional coupons of $t_B = 2$ mm and $I = 2w/3$ leads to $1/\alpha \approx (8t_F/3)^{1/4}$; therefore, $t_F \geq 3/8$ mm affects G_{DCB} at the level of 10% for the crack nucleation stage of $l \approx 10$ mm.

2.6. Fitting procedure for DCB test data

The crack-opening displacement in the DCB test was twice that of the lateral position $f_C(x)$ at loading point $x = 0$ in Eq. (18).

$$2f_C(0) = \frac{1}{3E_BI}\left[P_C\left\{2\left(\frac{1}{\alpha}+l\right)^3+\frac{1}{\alpha^3}\right\}+3M_C\left(\frac{1}{\alpha}+l\right)^2\right] \tag{33}$$

Moment M_C is approximated using Eq. (29) in a well-managed DCB test; hence, compliance $\lambda(l)_{DCB} = 2f_C(0)/P_C$ is expressed as follows:

$$\lambda(l)_{DCB} = \frac{1}{3E_BI}\left[\left\{2\left(\frac{1}{\alpha}+l\right)^3+\frac{1}{\alpha^3}\right\}-\frac{3P_C\left(\frac{1}{\alpha}+l\right)^4 L}{2\{E_BI+\left(\frac{1}{\alpha}+l\right)LP_C\}}\right] \tag{34}$$

When the hinge loading arm L decreases with $L \to 0$, Eq. (34) is simplified as follows:

$$\lambda(l)_{DCB,L\to 0} = \frac{1}{3E_BI}\left[\left\{2\left(\frac{1}{\alpha}+l\right)^3+\frac{1}{\alpha^3}\right\}+Erf\right] \tag{35}$$

where Erf is the error function. The coefficients $1/(3E_BI)$ and $1/\alpha$ in Eq. (35) were obtained by fitting the DCB test data $(\lambda_i, l_i), i = 1, 2, 3...n$ and applying the least-squares method when the error function Erf was negligible.

$$\Sigma\left\{\lambda_i - \lambda(l_i)_{DCB,L\to 0}\right\}^2 \to min. \tag{36}$$

Eq. (35) is simplified as follows when $1/\alpha l_i \to 0$:

$$\begin{aligned}\lambda(l_i)_{DCB,L\to 0} &= \frac{1}{3E_BI}\left[\left\{2\left(\frac{1}{\alpha}+l_i\right)^3+\frac{1}{\alpha^3}\right\}+Erf\right]\\ &\approx \frac{{l_i}^3}{3E_BI}\left\{2\left(1+\frac{1}{\alpha l_i}\right)^3+\left(\frac{1}{\alpha l_i}\right)^3\right\}\\ &\approx \frac{2{l_i}^3}{3E_BI}\left(1+\frac{3}{\alpha l_i}\right)\end{aligned} \tag{37}$$

Therefore, Eq. (36) can be expressed in a simplified form as follows:

$$\Sigma\left\{\lambda_i - \frac{2{l_i}^3}{3E_BI}\left(1+\frac{3}{\alpha l_i}\right)\right\}^2 \to min. \tag{38}$$

Eq. (38) is expressed as follows with coefficients $3/\alpha = A_5$ and $2/(3E_BI) = B_5$:

$$\Sigma\left(\lambda_i - B_5{l_i}^3 - A_5B_5{l_i}^2\right)^2 \to min. \tag{39}$$

For the partial differentiation of Eq. (39) for the coefficients A_5 and B_5 should be zero to be minimized. Therefore, the simultaneous equations for A_5 and B_5 are as follows:

$$\begin{cases}\Sigma(\lambda_i - B_5{l_i}^3 - A_5B_5{l_i}^2)(B_5{l_i}^2) = 0\\ \Sigma\left(\lambda_i - B_5{l_i}^3 - A_5B_5{l_i}^2\right)({l_i}^3 + A_5{l_i}^2) = 0\end{cases} \tag{40}$$

As $B_5 \neq 0$, Eq. (40) is simplified as follows:

$$\begin{cases}\Sigma\left(\lambda_i - B_5{l_i}^3 - A_5B_5{l_i}^2\right){l_i}^2 = 0\\ \Sigma\left(\lambda_i - B_5{l_i}^3 - A_5B_5{l_i}^2\right){l_i}^3 = 0\end{cases} \tag{41}$$

Therefore, the simultaneous equations in Eq. (41) yield the following solutions for A_5 and B_5.

$$\begin{cases}A_5 = \frac{3}{\alpha} = \frac{\Sigma{l_i}^6\Sigma\lambda_i{l_i}^2 - \Sigma{l_i}^5\Sigma\lambda_i{l_i}^3}{\Sigma{l_i}^4\Sigma\lambda_i{l_i}^3 - \Sigma{l_i}^5\lambda_i{l_i}^2}\\ B_5 = \frac{2}{3E_BI} = \frac{\Sigma{l_i}^4\Sigma\lambda_i{l_i}^3 - \Sigma{l_i}^5\Sigma\lambda_i{l_i}^2}{\Sigma{l_i}^4\Sigma{l_i}^6 - \Sigma{l_i}^5\Sigma{l_i}^5}.\end{cases} \tag{42}$$

Therefore,

$$\begin{cases}\frac{1}{\alpha} = \frac{\Sigma{l_i}^6\Sigma\lambda_i{l_i}^2 - \Sigma{l_i}^5\Sigma\lambda_i{l_i}^3}{3\left(\Sigma{l_i}^4\Sigma\lambda_i{l_i}^3 - \Sigma{l_i}^5\lambda_i{l_i}^2\right)}\\ \frac{1}{E_BI} = \frac{3\left(\Sigma{l_i}^4\Sigma\lambda_i{l_i}^3 - \Sigma{l_i}^5\Sigma\lambda_i{l_i}^2\right)}{2\left(\Sigma{l_i}^4\Sigma{l_i}^6 - \Sigma{l_i}^5\Sigma{l_i}^5\right)}.\end{cases} \tag{43}$$

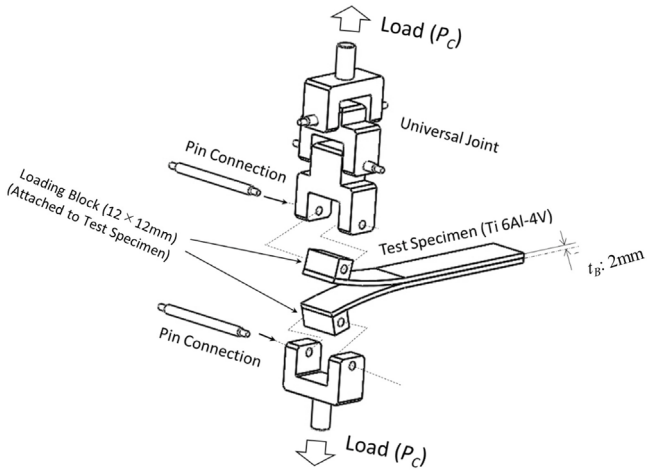

Fig. 7. DCB test setup:Overview.

The energy release rate $G_{DCB,L\to 0}$ was derived by substituting $E_B I$ and $1/\alpha$ into Eq. (32).

3. Experimental and discussions

The proposed method considers both the beam rotation and lateral movement at the crack front, and their comparisons are made with the MBT of the crack front rotation and simple beam theory (BT) of the fixed crack front.

The theoretical backgrounds of DCB test standards, such as ISO 15024, ASTM D5528, and JIS K7086, were not significantly different based on the MBT. JIS K7086 mainly introduces BT, and the crack-length correlation factor in MBT is determined by a linear plot between the cube root of the normalized compliance and normalized crack length. MBT is recommended in ASTM D5528 after round-robin testing with a compliance calibration method and a modified compliance calibration method, yielding a correlation factor Δ derived from a plot of $\lambda^{1/3}$ versus crack length l. The energy release rate G_{DCB} and Young's modulus of beam E_B were determined in the MBT of ASTM D5528 as follows:

$$G_{DCB} = \frac{3P_C\delta}{2w(l+|\Delta|)} \tag{44}$$

$$E_B = \frac{64P_C(l+|\Delta|)^3}{\delta w(2t_B)^3} \tag{45}$$

In crack inspection, JIS K7086 accepts temporal unloading to stop crack propagation for intensive checks, rendering GVI in many cases, acceptably accurate in measuring crack length l. Therefore, JIS K7086 was adopted for the DCB testing on a Ti-6Al-4V plate (Standard Test Piece, Japan), 150 mm along the crack elongation direction, 25 mm in width, and 2 mm in average thickness, bonded with an FM 309 film adhesive (Solvay, USA), as shown in Fig. 7.

The Ti-6Al-4V plates were surface-treated for bonding as follows: degreased with FineSoleve E acetone-substituting detergent (Sankyo Chemical Co., Japan), sandblasted with Fuji Rundum WA SMAWF080 Al_2O_3 powder–150–212 μm in diameter (Fuji Manufacturing, Japan), and boiled in purified water for 30 min to stabilize the surface conditions. The autoclave was set at 183.0 °C for 140 min to cure the specimen with a 40 mm film crack of 12.5 μm thick Kapton film (DuPont, USA). A 12 mm square loading block was attached for the DCB testing of samples No. 1 to 5 using a Shimadzu Autograph AG-X tensile test machine (Shimadzu SLBL 1kN type Shimadzu Autograph AG-X) , as shown in Fig. 8, with the cross-head speed of 1.0 mm/min.

The specimen sides were coated in white for GVI to increase the visual contrast of the dark-appearing cracks caused by the white coating, as depicted in Fig. 9.

Fig. 10 shows the crosshead displacement–load curves. The crosshead displacements were correlated with the zero positions using linear fitting, as shown in Fig. 10 to determine the compliance for the BT and MBT methods.

Moment M_C caused by the hinge loading arm $L = 7$ (mm), which is half that of the loading block of 12 mm and Ti-6Al-4V plate thickness of 2 mm, as shown in Fig. 8, was two to three digits smaller and thus regarded negligible against the lateral load P_C with Eq. (29), as presented in Table 1.

The crack length correlation factor Δ in MBT was defined by applying a linear relationship between crack length l and $\lambda^{1/3}$ as depicted in Fig. 11.

The calculated energy release rates, excluding the data points of the unstable fracture cases, were compared between the BT (JIS K7086) method, MBT (ASTM D5528) for Eq. (44) and the proposed method for Eqs. (32) and (43), as presented in Fig. 12 and Table 2.

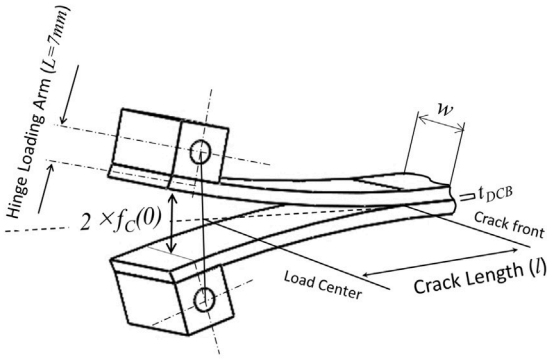

(a) Crack Region: Notation

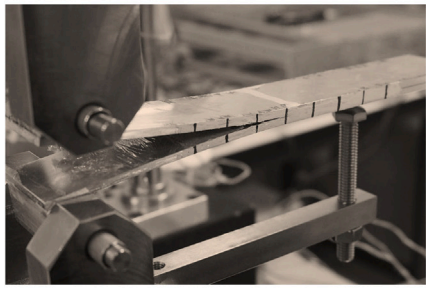

(b) Crack Region Overview

Fig. 8. DCB test setup: Crack region zoom up.

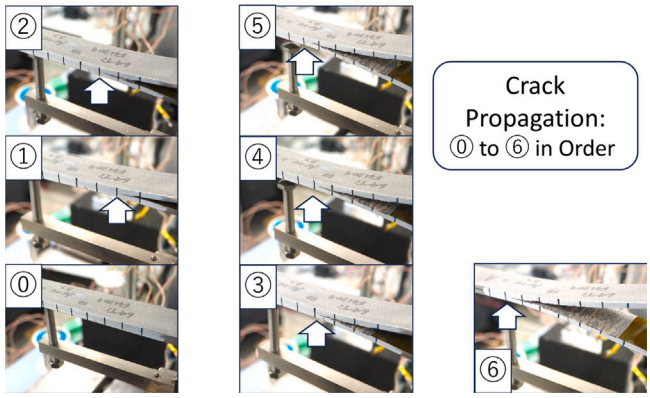

Fig. 9. GVI for the crack propagation in DCB Test.

Table 1
Moment by Hinge loading arm $L = 7$ mm.

Lateral Load P_C($\times 10^2$ N)	Moment ($\times 10^{-1}$ Nm)
1.99	1.15
1.66	1.24
1.41	1.28
1.11	1.08
1.02	1.18
0.85	1.04
0.82	1.19
0.70	1.04

The energy release rate calculations presented in Table 2 demonstrate that the proposed DCB test method provides a significantly smaller standard deviation than the current BT method in JIS K7086. Furthermore, as shown in Fig. 12, the BT method shows a sloped value on the overestimation side for the crack nucleation and propagation stages and underestimation side for the final stage of a long crack. Conversely, the influence of the crack length was small in the proposed method; thus, the proposed method is expected to provide more reliable values than the BT method.

The MBT method in ASTM D5528 demonstrated the calculated energy release rates with the smallest standard deviation and the most conservative side. Therefore, the MBT is recommended for engineering applications requiring high reproducibility and a large structural safety margin. However, the crack length correlation factors $|\Delta|$ appear large in the values while MTB in ASTM D5528 assumes the case $l + |\Delta|$ is slightly longer than l; therefore, the soundness of the MBT may be elusive in this experiment.

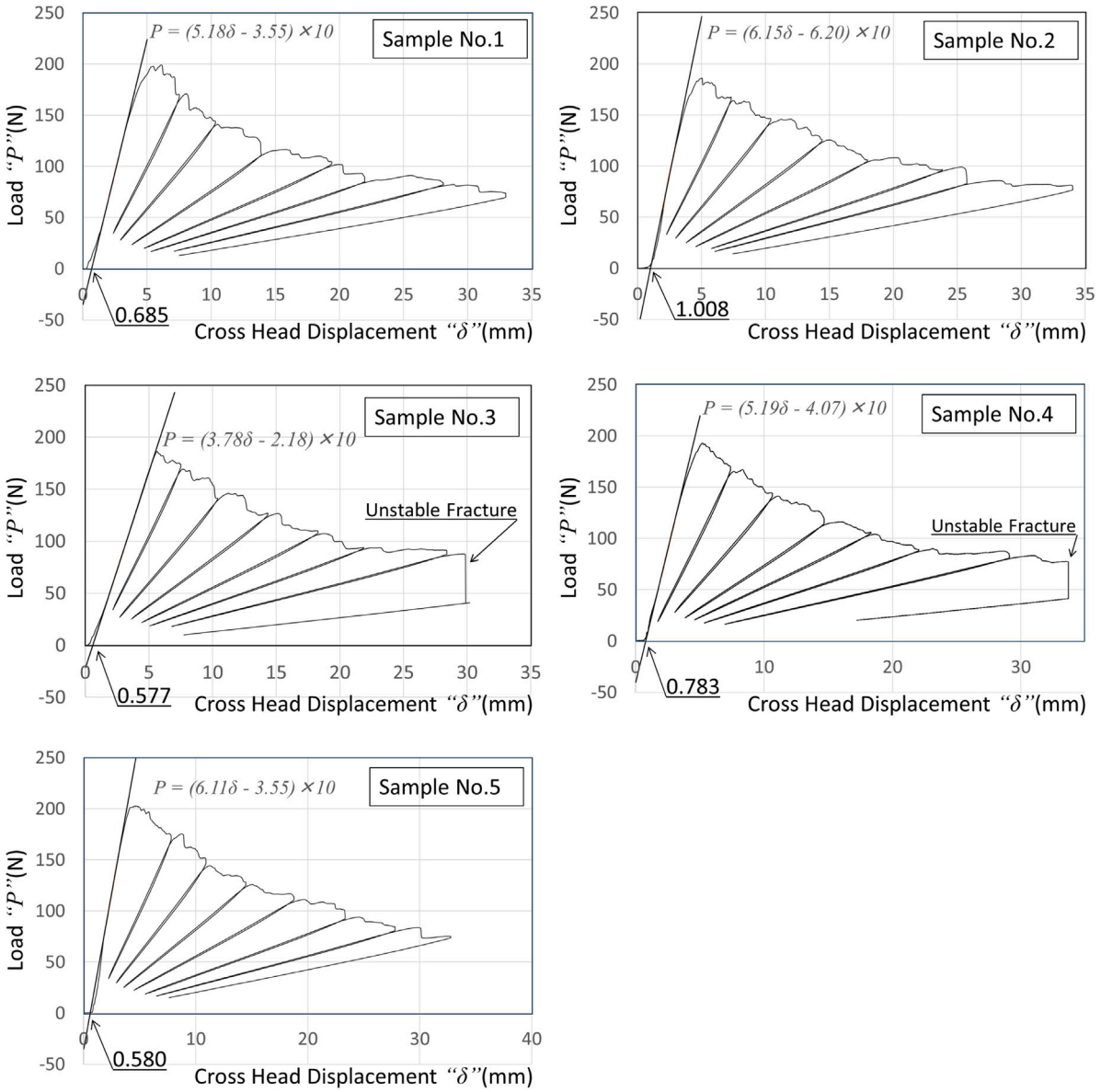

Fig. 10. Displacement-load curves.

The proposed method and the MBT method demonstrated a good agreement for the E_Bs of ±10% in the distributions and the average values within 5%; therefore, the CFs of $1/\alpha$ is expected to reflect the robustness of the crack front treatment.

3.1. Method selection in DCB test

The three methods, BT, MBT, and the proposed method, treat the crack front as follows:

· **BT method**: Rigid clamp. The lateral movement of the loading point is given by the Bernoulli–Euler beam theory.

· **MBT method**: Rotation is considered. The lateral movement of the loading point is given by the Bernoulli–Euler beam theory, and the slope at the crack front multiplied by crack length.

· **Proposed method**: Both rotation and lateral movement are considered. The lateral movement of the loading point is given by the Bernoulli–Euler beam theory, the slope at the crack front multiplied by the crack length, and lateral movement at the crack front.

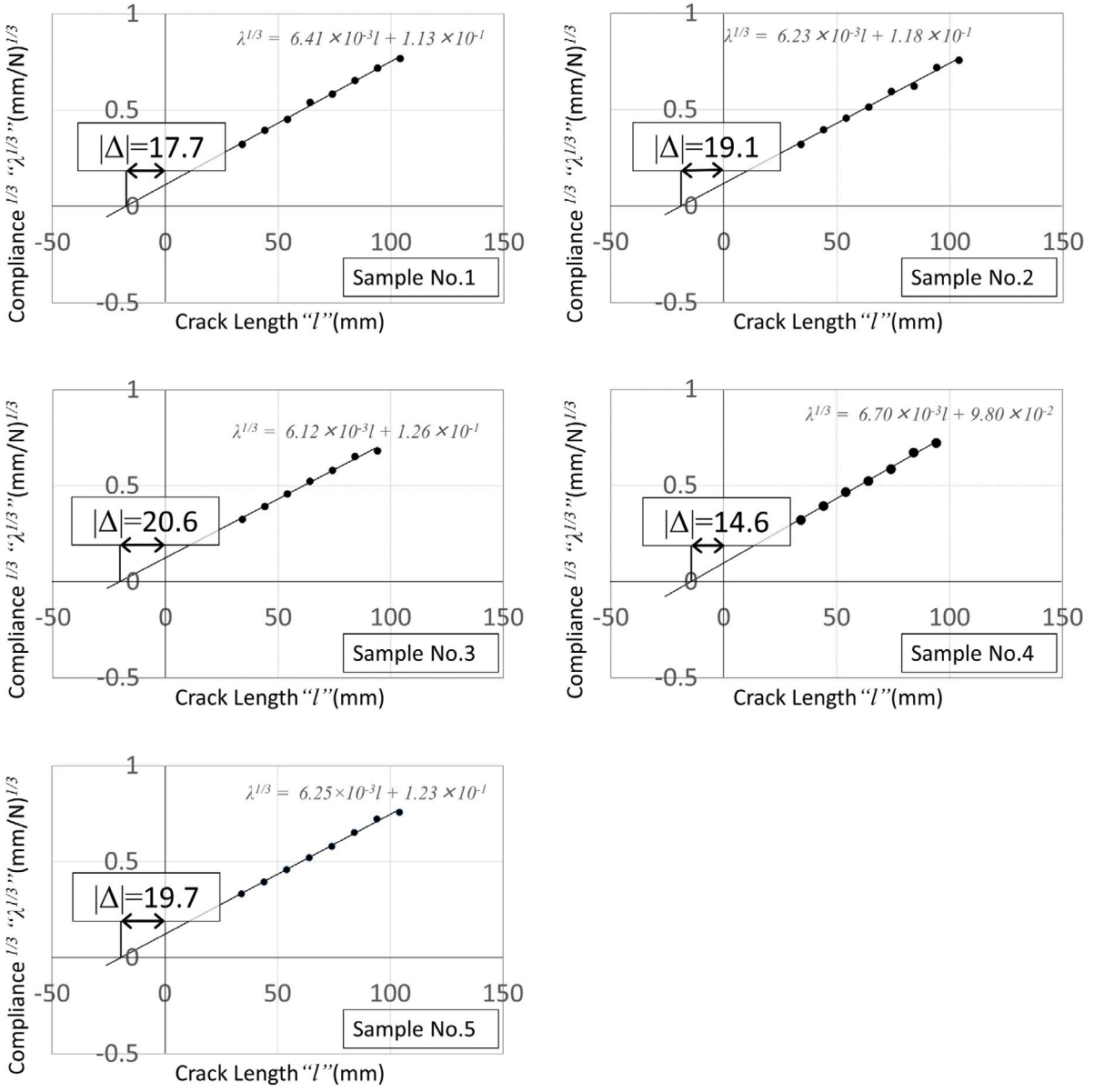

Fig. 11. Crack length correlation factor Δ for Modified Beam Theory.

Therefore, the proposed method is expected to be less effective than the MBT method when the lateral movement is negligible, and the simple BT method becomes acceptable when the crack-front rotation triggers a negligible effect. Therefore, it is reasonable to select a method that uses two parameters; R_{MBT} and R_{BT}, as follows:

· **Selection: Proposed method**, when $R_{MBT} \nrightarrow 0$.

· **Selection: MBT method**, when $R_{MBT} \to 0$.

· **Selection: BT method**, when $R_{BT} \to 0$.

$$R_{MBT} \equiv \left\{ f(l) / \left(-l \left[\frac{\partial f(x)}{\partial x} \right]_{x=l} \right) \right\} = \frac{1+\alpha l}{\alpha l(1+2\alpha l)} \tag{46}$$

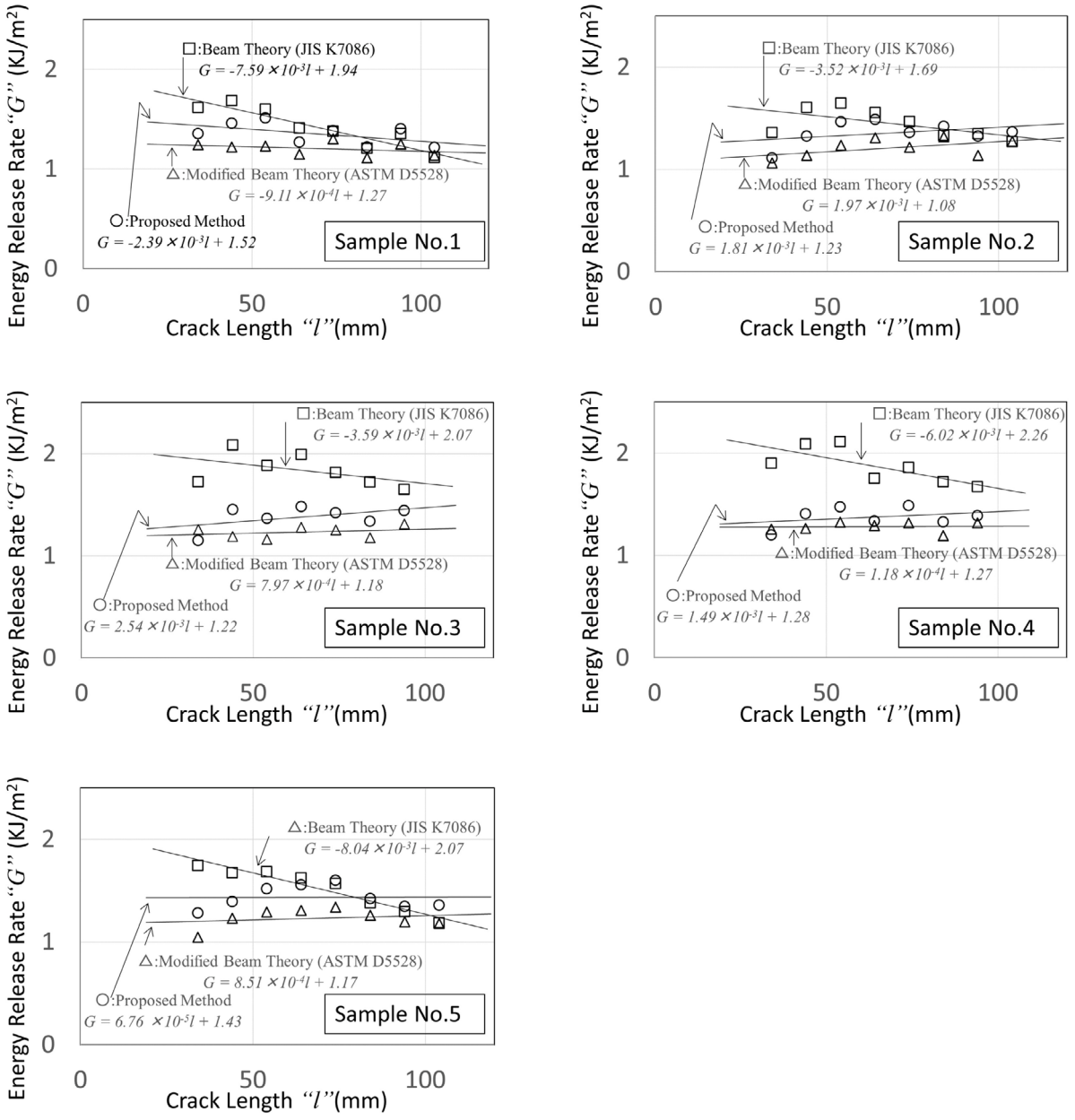

Fig. 12. R-Curves.

$$R_{BT} \equiv \frac{-l\left[\frac{\partial f(x)}{\partial x}\right]_{x=l}}{P_C l^3/(3E_B I)} = \frac{3(1+2\alpha l)}{2(\alpha l)^2} \tag{47}$$

where the lateral movement at the crack front is expressed by Eq. (15) as $f(l)$, the rotation at the crack front is given in Eq. (17) as $\left[\frac{\partial f(x)}{\partial x}\right]_{x=l}$, and $P_C l^3/(3E_B I)$ is the lateral bending in Bernoulli–Euler beam theory.

Fig. 13 depicts the case when R_{MBT} and R_{BT} are 0.1, where $f(l)$ provides 10% level error over $-l\left[\frac{\partial f(x)}{\partial x}\right]_{x=l}$ and $-l\left[\frac{\partial f(x)}{\partial x}\right]_{x=l}$ over $P_C l^3/(3E_B I)$, yielding $\alpha l \approx 5.42$ and $\alpha l \approx 30.5$. In this experiment, $1/\alpha$ ranged from 5.11 to 10.1, as summarized in Table 2;

Table 2
Experimental results.

Sample No.	Energy Release Rate (kJ/m^2)			CF(mm)	E_B (GPa)	t_{DCB}
		Average	S.D.($\times 10^{-1}$)	$1/\alpha(Top)$, $\lvert\Delta\rvert$(Middle)		(mm)
1	Proposed Method	1.35	1.02	7.92	118	0.611
	MBT(ASTM D5528)	1.21	0.606	17.7	118	–
	BT(JIS K7086)	1.42	1.89	–	–	–
2	Proposed Method	1.36	1.09	8.23	128	0.571
	MBT(ASTM D5528)	1.21	0.858	19.1	134	–
	BT(JIS K7086)	1.44	1.32	–	–	–
3	Proposed Method	1.38	1.05	10.1	136	0.649
	MBT(ASTM D5528)	1.23	0.521	20.7	135	–
	BT (JIS K7086)	1.89	1.45	–	–	–
4	Proposed Method	1.26	3.20	5.23	111	0.536
	MBT(ASTM D5528)	1.21	1.92	14.6	113	–
	BT(JIS K7086)	1.87	1.62	–	–	–
5	Proposed Method	1.45	1.08	5.11	113	0.631
	MBT(ASTM D5528)	1.23	0.868	19.8	133	–
	BT(JIS K7086)	1.52	1.92	–	–	–
			(S.D. of Sample Averages)			
Average of 1 to 5	Proposed Method	1.36	0.610	7.32	121	0.600
	MBT(ASTM D5528)	1.22	0.0970	18.4	127	–
	BT(JIS K7086)	1.63	2.09	–	–	–

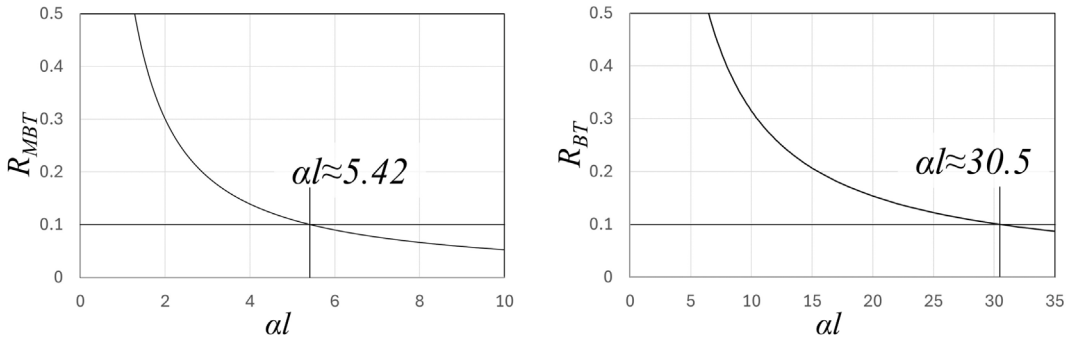

(a) Selection on Modified Beam Theory (b) Selection on Beam Theory

Fig. 13. DCB test method selection parameters.

therefore, the proposed method is recommended when the crack length $l < 54.7$(mm) and MBT is recommended over BT when $l < 308$(mm), which is true because of the limitation of the specimen length, that is, 150 mm.

Therefore, the existing BT or MBT methods provide an acceptable option when the limitation in the crack length l is not an issue in DCB testing; however, the proposed method provides a reasonable option when l is limited owing to engineering requirements, such as DCB testing for the crack initiation stage and assessment of nondestructive testing if the detection limit of l is acceptable.

4. Conclusions

We propose a modified DCB test method to consider the infinitesimal deformation of a slender beam on Winkler's elastic foundation, assuming that the beam deformation is predictable using the Bernoulli–Euler beam model. Moreover, the crack-end deformation was determined using both the slope and lateral movement of Winkler's elastic foundation, yielding an energy release rate with a foundation-based correlation factor for the crack length.

The modified method was assessed based on the DCB test results of Ti6Al4V samples, showing reasonable consistency, particularly for the short cracking of the nucleation and growth stages of the energy release rate.

CRediT authorship contribution statement

Tetsuya Morimoto: Writing – original draft, Visualization, Validation, Supervision, Resources, Project administration, Methodology, Investigation, Funding acquisition, Formal analysis, Data curation, Conceptualization. **Hisaya Katoh:** Methodology, Investigation. **Yuichi Ishida:** Methodology, Investigation. **Eiichi Hara:** Methodology, Investigation. **Masahiro Kusano:** Validation, Investigation, Funding acquisition, Conceptualization. **Kimiyoshi Naito:** Investigation, Funding acquisition, Conceptualization. **Makoto Watanabe:** Funding acquisition, Conceptualization. **Kiyoka Takagi:** Project administration, Funding acquisition, Conceptualization. **Keiji Arai:** Project administration, Funding acquisition, Conceptualization. **Koichi Hasegawa:** Methodology, Investigation, Conceptualization.

Declaration of competing interest

The authors declare the following financial interests/personal relationships which may be considered as potential competing interests: Tetsuya Morimoto reports financial support was provided by Acquisition Technology and Logistics Agency. If there are other authors, they declare that they have no known competing financial interests or personal relationships that could have appeared to influence the work reported in this paper.

Data availability

Data will be made available on request.

Acknowledgments

This study was supported by the Innovative Science and Technology Initiative for Security Grant Number JPJ004596, ATLA Japan. We would like to thank Editage (www.editage.jp) for the English language editing.

Appendix A. Energy release rate of extreme-long hinge loading arm case

For the extreme case of the hinge loading arm L as $L \to \infty$, Eq. (31) can be simplified as follows:

$$G_{DCB,L\to\infty} = \frac{{P_C}^2}{4wE_BI}\left(\frac{1}{\alpha}+l\right)^2 \tag{A.1}$$

The case in Eq. (A.1) is equivalent to a DCB test with the crack-tip rotation $\left[\frac{\partial f_C(x)}{\partial x}\right]_{x=0}$ constrained to zero, which is realized for half of the center-cracked double beam, as shown in Fig. A.1 or by using rotation-constraining gripping, as shown in Fig. A.2.

In addition, Eq. (34) is simplified as follows.

$$\begin{aligned}\lambda(l_i)_{DCB,L\to\infty} &= \frac{1}{3E_BI}\left[\left\{2\left(\frac{1}{\alpha}+l_i\right)^3+\frac{1}{\alpha^3}\right\}-\frac{3}{2}\left(\frac{1}{\alpha}+l_i\right)^3+Erf\right]\\ &\approx \frac{{l_i}^3}{3E_BI}\left\{\frac{1}{2}\left(1+\frac{1}{\alpha l_i}\right)^3+\left(\frac{1}{\alpha l_i}\right)^3\right\}\\ &\approx \frac{1{l_i}^3}{6E_BI}\left(1+\frac{3}{\alpha l_i}\right)\end{aligned} \tag{A.2}$$

Therefore, coefficients $1/\alpha$ and $1/(E_BI)$ are obtained as follows:

$$\begin{cases}\dfrac{1}{\alpha} = \dfrac{\Sigma {l_i}^6 \Sigma \lambda_i {l_i}^2 - \Sigma {l_i}^5 \Sigma \lambda_i {l_i}^3}{3\left(\Sigma {l_i}^4 \Sigma \lambda_i {l_i}^3 - \Sigma {l_i}^5 \lambda_i {l_i}^2\right)}\\ \dfrac{1}{E_BI} = \dfrac{6\left(\Sigma {l_i}^4 \Sigma \lambda_i {l_i}^3 - \Sigma {l_i}^5 \Sigma \lambda_i {l_i}^2\right)}{\left(\Sigma {l_i}^4 \Sigma {l_i}^6 - \Sigma {l_i}^5 \Sigma {l_i}^5\right)}.\end{cases} \tag{A.3}$$

The energy release rates $G_{DCB,L\to\infty}$ were derived by substituting E_BI and $1/\alpha$ into Eq. (A.1).

Appendix B. Crack inspection in DCB test

In many cases, GVI provides acceptable accuracy in measuring the length of stable cracks in temporal unloading in JIS K7086, if needed, with the aid of increasing the visual contrast of dark cracks by white coating of the specimen sides, as depicted in Fig. 9 or using a microscope as shown in Fig. B.1.

When temporal unloading is not accepted, the crack gauge provides an option for DVI of the crack length in real time. Crack gauges were set on the two sides of the DCB specimen to provide the average crack length, as depicted in Fig. B.2. The propagating crack cut the grid wire to shift the gauge resistance and drifted the output potential to appear in a stepwise manner, as shown in Fig. B.3, providing the crack length as the step numbers times the grid pitch.

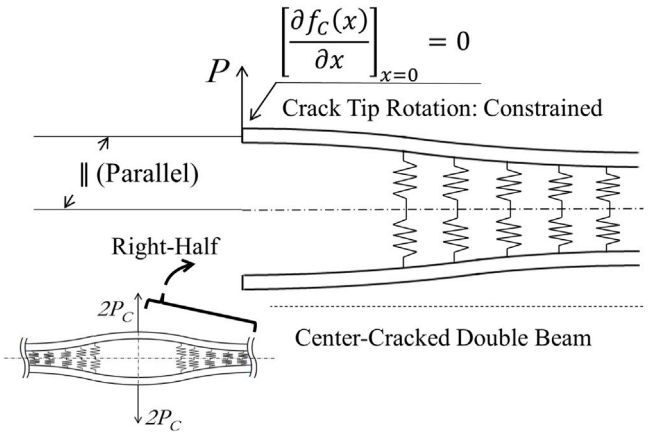

Fig. A.1. Model for extreme-long hinge loading arm case.

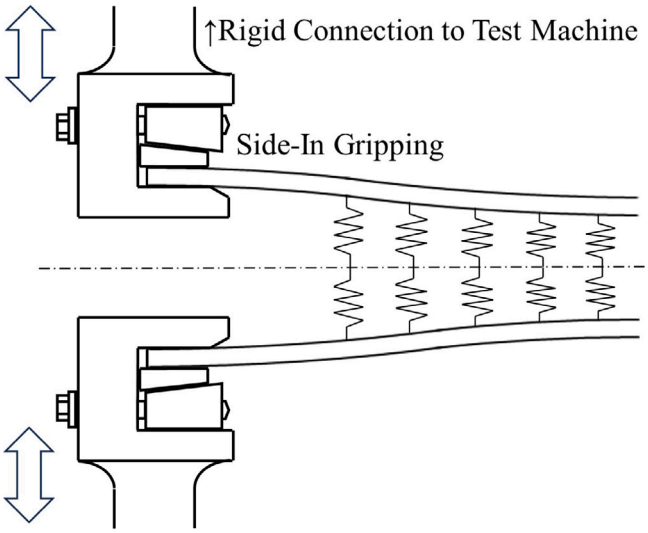

Fig. A.2. Example of rotation constraining gripping.

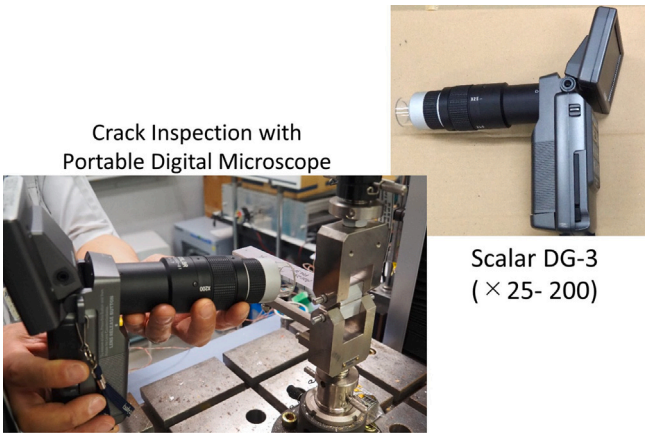

Fig. B.1. Microscopic inspection in DCB test.

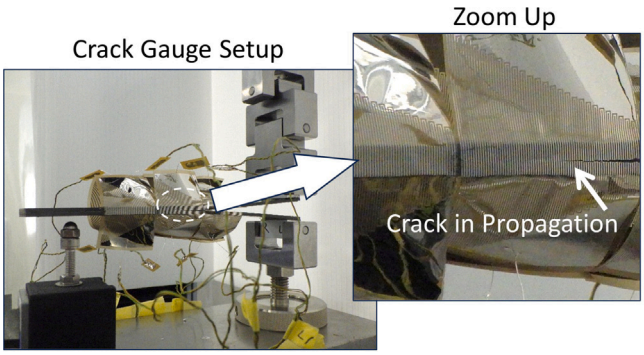

Fig. B.2. Crack gauge setup in DCB test.

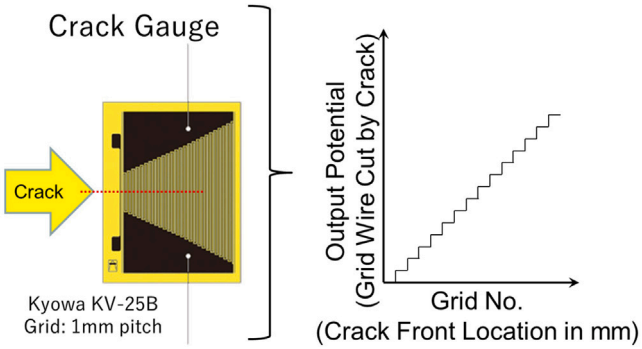

Fig. B.3. Crack gauge overview.

References

[1] Imperiale VA, Cosentino E, Weaver PM, Bond IP. Compound joint: A novel design principle to improve strain allowables of FRP composite stringer run-outs. Composites A 2010;41:521–31.
[2] Navas SH, Huete SC, Menendez JGI, Hidalgo AA. Assignee: AIRBUS OPERATIONS S.I. In: Load transfer devices at a stringer run-out. United States Patent Application Publication; 2012, Pub. No. US 2012/0234978 A1.
[3] Transportation Safety Board of Canada. Loss of rudder in flight airbus 310-308 C-GPAT Miami, Florida, 90 nm S 06 2005. In: Aviation investigation report A05F0047. 2005.
[4] Federal Aviation Administration (FAA), Aviation Rulemaking Advisory Committee (ARAC), Transport Airplane Metallic and Composite Structures Working Group. Transport airplane metallic and composite structures working group – recommendation report to FAA structural bonding. 2021.
[5] Federal Aviation Administration (FAA), Advisory Circulars. AC 20-107B - Composite aircraft structure. 2009.
[6] ISO15024:2023(E). Fibre-reinforced plastic composites-Determination of mode I interlaminar fracture toughness, G_{IC}, for unidirectionally reinforced materials.
[7] ASTMD5528/D5528M-21. Standard Test Method for Mode I Interlaminar Fracture Toughness of Unidirectional Fiber-Reinforced Polymer Matrix Composites.
[8] ASTMD3433-99. Standard Test Method for Fracture Strength in Cleavage of Adhesives in Bonded Metal Joints.
[9] JISK7086-1993. Testing methods for interlaminar fracture toughness of carbon fibre reinforced plastics.
[10] Akhavan-Safar A, Beygi R, Delzendehrooy F, da Silva LFM. Fracture energy assessment of adhesives - part I: Is G_{IC} an adhesive property? A neural network analysis. J Mater Des Appl 2021;235(6):1461–76.
[11] Bisshopp KE, Drucker DC. Large deflection of cantilever beams. Quart Appl Math 1945;III(3):272–5.
[12] Devitt DF, Schapery RA, Bradley WL. A method for determining the mode I delamination fracture toughness of elastic and viscoelastic composite materials. J Compos Mater 1980;14:270–85.
[13] NASA Reference Publication, 1092. Standard tests for toughened resin composites. 1983, p. 25–35.
[14] Wang SS, Suemasu H, Zahlan NM. Interlaminar fracture of random short-fiber SMC composite. J Compos Mater 1984;18:574–94.
[15] Williams JG. On the calculation of energy release rates for cracked laminates. Int J Fract 1988;36:101–19.
[16] Berry JP. Determination of fracture surface energies by the cleavage technique. J Appl Phys 1963;34(1). 62–68.
[17] Kageyama K, Kobayashi T. An interlaminar fracture toughness test in mode I for composite laminates. J Jpn Soc Compos Mater 1987;13(6):265–70.
[18] Kageyama K, Kobayashi T, Nonaka K. Mode I interlaminar fracture mechanics of unidirectionally reinforced carbon/epoxy laminates. Trans JSME(A) 1987;53(494):1898–904.
[19] Kageyama K, Kobayashi T, Yanagisawa N, Kikuchi M, Miyamoto H. Mode I interlaminar fracture mechanics of unidirectionally reinforced carbon/nylon laminates. Trans JSME(A) 1987;53(496):2386–93.
[20] Kageyama K, Kimpara I, Ohsawa I, Hojo M. Damage tolerance estimation of advanced composite materials - 1st report : Study on interlaminar fracture toughness test. J Soc Nav Archit Jpn 1990;1990(168):497–506.
[21] Winkler E. Vortraege ueber Eisenbahnbau. 1867, Heft 1, 2. H. Dominicus, Prag.
[22] Winkler E. Die Lehre von der Elasticitaet und Festigkeit. 1867, Theil 1 2. H. Dominicus, Prag.
[23] Biot MA. Bending of an infinite beam on an elastic foundation. J Appl Mech 1937;A–1–A–7.

[24] Pavlović MN, Tsikkos S. Beams on Quasi-Winkler foundations. Eng Struct 1982;4:113–8.
[25] Kanninen MF. An augmented double cantilever beam model for studying crack propagation and arrest. Int J Fract 1973;9(1):83–92.
[26] Kanninen MF. A dynamic analysis of unstable crack propagation and arrest in the DCB test specimen. Int J Fract 1974;10(3):415–30.
[27] Whitney JM. Stress analysis of the double cantilever beam specimen. Compos Sci Technol 1985;23:201–19.
[28] Williams JG. End corrections for orthotropic DCB specimens. Compos Sci Technol 1989;35:367–76.
[29] Williams JG. The fracture mechanics of delamination tests. J Strain Anal 1989;24(4):207–14.
[30] Kondo K. Analysis of double cantilever beam specimen. Adv Compos Mater 1995;4(4):355–66.
[31] Shokrieh MM, Heidari-Rarani M. A comparative study for beams on elastic foundation models to analysis of mode-I delamination in DCB specimens. Struct Eng Mech 2011;37(2):149–62.
[32] Takeda T. Mode I fracture toughness determination and environmental durability evaluation of adhesive bonds by wedge test. Int J Adhes Adhes 2023;127:1–11.
[33] Cabello M, Turon A, Zurbitu J, Renart J, Sarrado C, Martinez F. Progressive failure analysis of DCB bonded joints using a new elastic foundation coupled with a cohesive damage model. Eur J Mech A Solids 2017;63:22–35.
[34] Mantic V, Vazquez-Sanchez A, Romero-Laborda M, Munoz-Reja M, Jimenez-Alfaro S, Tavara L. A new crack-JTip element for the logarithmic stress-singularity of mode-III cracks in spring interfaces. Comput Mech 2024. http://dx.doi.org/10.1007/s00466-024-02448-6.